JOURNAL OF THE AERONAUTICAL SCIENCES

VOLUME 21 JULY, 1954 NUMBER 7

Measurements of Turbulent Friction on a Smooth Flat Plate in Supersonic Flow*

DONALD COLES†

California Institute of Technology

SUMMARY

Direct measurements of supersonic local skin friction, using the floating-element technique, are presented for Mach Numbers from 2.0 to 4.5 and Reynolds Numbers from 3×10^5 to 9×10^6. Turbulent flow and transition are emphasized, although some measurements in the laminar regime are included. The observed effect of compressibility is to reduce the magnitude of turbulent skin friction by a factor of two at a Mach Number of 4.5 and a Reynolds Number of about 10^7.

The boundary-layer momentum-integral equation for constant pressure is verified within a few per cent by two experimental methods. Typical static pressure measurements are presented to show that transition can be detected by observing disturbances in pressure associated with changes in displacement thickness of the boundary layer.

It is found that the turbulent boundary layer cannot be defined experimentally for values of $u_1\theta/\nu_1$ less than about 2,000, where θ is the momentum thickness. For larger values of $u_1\theta/\nu_1$ there is a unique relationship between local friction coefficient and momentum-thickness Reynolds Number at a fixed Mach Number. The Appendix compares the present measurements at $M = 2.5$ with experimental data from other sources.

INTRODUCTION

THE FLOATING-ELEMENT TECHNIQUE, which attempts to measure directly the friction drag on a portion of a body in a fluid flow, was successfully used in 1929 by Kempf[1] and later by Schultz-Grunow.[2] An early but largely unproductive effort to apply the technique at supersonic speeds was that of Ginsburgh.[3] Beginning in 1948, H. W. Liepmann at GALCIT‡ undertook the development of a floating-element instrument for high-speed flow, and this work has been carried forward by Dhawan[4] and by Hakkinen.[5] The method has also been used, with variations, by Weiler and Hartwig[6] at the University of Texas, by Eimer[7] at GALCIT, by Bradfield, DeCoursin, and Blumer[8] at the University of Minnesota, and with conspicuous success by Chapman and Kester[9] at the Ames Aeronautical Laboratory of the NACA, the last two of these investigations being made with a body of revolution rather than with a flat-plate model.

The writer's research at JPL,** although inspired by the success of Liepmann and his group, is an independent attack on the flat-plate drag problem. During the research full advantage was taken of the size and range of the 20-in. supersonic wind tunnel at the Jet Propulsion Laboratory and of Liepmann's experience with the floating-element technique. Design of the flat-plate model and instrumentation was begun in early 1951, and the experiments discussed here were carried out in the spring of 1952. The present research has been briefly reported at the 1952 Annual Summer Meeting of the Institute of the Aeronautical Sciences in Los Angeles and at the Eighth International Congress on Theoretical and Applied Mechanics in Istanbul, and some preliminary data have been published in a short note.[10] A comprehensive discussion of the research can be found in the writer's thesis,[11] which has been published in three reports of the Jet Propulsion Laboratory.[12–14] Some introductory remarks in the thesis have also appeared as a survey paper.[15]

LIST OF SYMBOLS

C_f = local friction coefficient
C_F = mean friction coefficient

Received December 22, 1953.

* This paper presents the results of one phase of research carried out at the Jet Propulsion Laboratory, California Institute of Technology, under joint sponsorship of the Department of the Army, Ordnance Corps (under Contract No. DA-04-495-Ord 18), and the Department of the Air Force.

† Research Engineer, Jet Propulsion Laboratory; now Research Fellow.

‡ Guggenheim Aeronautical Laboratory, California Institute of Technology.

** Jet Propulsion Laboratory, California Institute of Technology.

M = free-stream Mach Number
p = pressure
q = free-stream dynamic pressure, $\rho_1 u_1^2/2$
R = ideal Reynolds Number
R' = Reynolds Number per unit length, u_1/ν_1
R_t = ideal Reynolds Number corresponding to point of observed maximum surface shearing stress
R_θ = momentum-thickness Reynolds Number, $u_1\theta/\nu_1$
T = temperature
u = velocity
x = distance from plate leading edge
y = distance from plate surface
γ = ratio of specific heats
δ = boundary-layer thickness
δ^* = boundary-layer displacement thickness
θ = boundary-layer momentum thickness
θ_0 = momentum-thickness increment of tripping device
μ = viscosity
ν = kinematic viscosity, μ/ρ
ρ = density
τ_w = wall shearing stress

Subscripts

0 = value at stagnation condition
1 = value in free stream
i = value for $M = 0$ at fixed R

Model and Instrumentation

(1) *Flat Plate*

Fig. 1 shows the flat-plate model installed in the test section of the 20-in. supersonic wind tunnel at the Jet Propulsion Laboratory. The plate completely spanned the tunnel in order to isolate the working surface from disturbances originating elsewhere on the model. Three floating-element instruments were mounted in the plate, on the tunnel plane of symmetry, at $x = 5.5$, 13.0, and 24.0 in. from the leading edge. Three small windows of $^1/_2$-in. plate glass were installed in each door, so that flow over the plate surface and leading edge could be observed using the tunnel schlieren system.

A series of static-pressure orifices was provided on the plate surface about 3 in. from the tunnel centerline. In addition, each of the floating-element instruments incorporated three orifices for static-pressure measurement; one of these orifices was the gap around the element itself. Three copper-constantan thermocouples were soldered to stainless-steel buttons buried in the plate surface near the floating-element stations, and the temperature was also measured in the element balance chambers and in the tunnel reservoir.

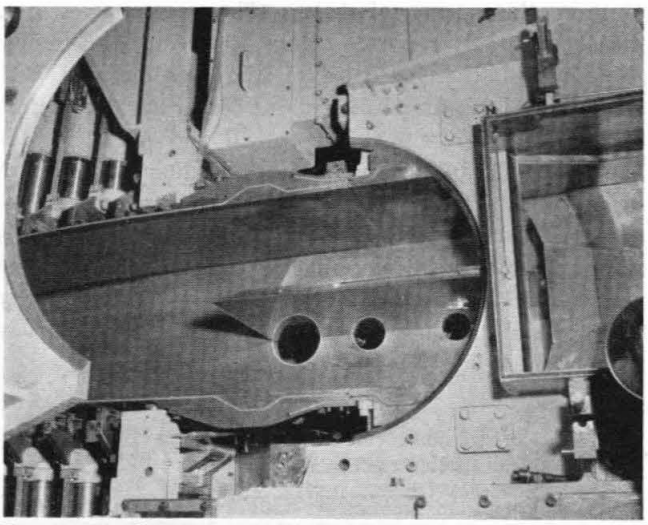

FIG. 1. The flat-plate model in the 20-in. supersonic wind tunnel.

All metal components exposed to the air stream on the working surface of the plate were fabricated of stainless steel. Particular attention was paid to working-surface finish and to the sharpness of the leading edge, which was a wedge of 15-deg. included angle. Various methods of estimating the leading-edge radius indicated that the value finally achieved was less than one half-thousandth of an inch.

(2) *Floating Element*

The skin-friction instrument used at JPL was similar in principle to the floating-element mechanism of Liepmann and Dhawan.[4] The most important difference, aside from size and range, was the use at JPL of a null technique in measuring applied forces.

The basic components of the instrument are shown in Figs. 2 and 3. The inner flexure system, consisting of the table, two flexlinks, and the ring, allowed a deflection of the element under an applied load. The deflection was measured indirectly as the displacement that must be given to the table in order to return the element to a standard null position with respect to the surrounding structure. Motion of the table was effected by means of a precision micrometer, acting through a piano-wire push rod clamped at both ends, and was constrained by the second or outer flexure system shown in the figures.

The null position of the floating element was detected by a Schaevitz variable-reluctance transformer[16] whose coil was fixed on the instrument structure and whose core was attached to the element ring. Two dashpots were provided for damping in the inner flexure system and were adjusted to give slightly less than critical damping. The choice of a rectangular surface element was made in order to approximate a local measurement, and the corresponding rectangular hole, $^1/_4$ by $1^1/_2$ in., was fabricated by a combination of milling, machine-filing, and broaching operations.

(3) *Micrometer*

The micrometer shown in Figs. 2 and 3 was designed around a standard commercial lead-screw of 0.025-in. pitch. The lead-screw was keyed to prevent rotation and was actuated by a rotating nut that was driven through a worm and worm gear. A counter and graduated dial on the micrometer input shaft indicated the position of the lead-screw in millionths of an inch.

Each of the micrometers was calibrated by direct comparison with a Pratt & Whitney standard measuring machine. It was found that the maximum micrometer position error did not exceed 0.5 per cent and so

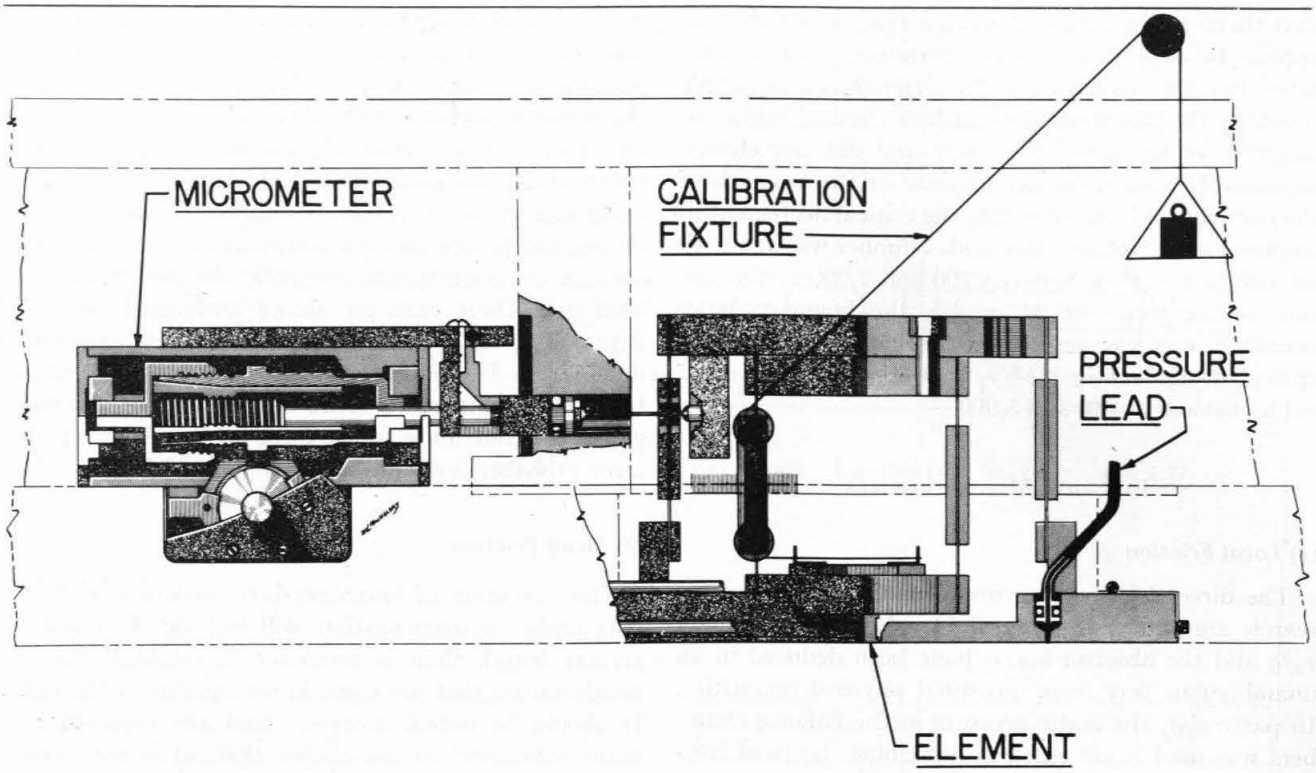

FIG. 2. The floating element and micrometer installed in the plate.

could be neglected in the present measurements. In general, under steady conditions, the null position as indicated by the Schaevitz gage could be repeated within one or two millionths of an inch using ordinary care to avoid backlash in the mechanism of the micrometer. Failure to obtain the sensitivity mentioned could usually be traced to the presence of foreign material in the clearance gaps. The spring constant for the inner flexure system was about 0.4 lb. per in., and deflections ranging from 0.0005 to 0.015 in. were encountered in the wind tunnel.

(4) Tripping Devices

During the JPL research, three different tripping devices were used to stimulate transition to turbulent flow. These were a sand strip, a leading-edge fence, and a row of airjets. The fence, consisting of a row of wire posts normal to the airflow and to the plate surface, was used in most of the measurements of turbulent friction. The sand strip was tested at $M = 4.5$, and the effect of air discharge on transition was investigated at Mach Numbers of 2.0 and 4.5. Fig. 4 shows the appearance of the boundary-layer flow at $M = 4.5$ with natural transition and with the various tripping devices.

The fence was found to have the virtue that the initial momentum loss at the wires could be computed from the known drag characteristics of cylinders in supersonic flow. However, there is some doubt as to whether true equilibrium was reached in the turbulent boundary layer far downstream, where the fence usually contributed from 10 to 20 per cent of the total momentum loss. The wires used were 0.014 in. in diameter, spaced $^1/_4$ in. apart, and projected about $^1/_{10}$ in. beyond the surface of the plate. For increasing Mach Number, there was a small but noticeable increase in the wire Reynolds Number needed to trip the boundary layer.

The device of discharging air from small holes in a surface was proposed by Fage and Sargent[17] as a method of stimulating transition to turbulent flow in the boundary layer. The most important property of such a tripping device, aside from the obvious advantage of control, is the small intrinsic drag of the jets. In the JPL tests, air was discharged from a row of holes 0.014 in. in diameter, spaced $^1/_4$ in. apart, and located $^3/_4$ in. from the leading edge. During some preliminary measurements at a Mach Number of 2.0, it was found

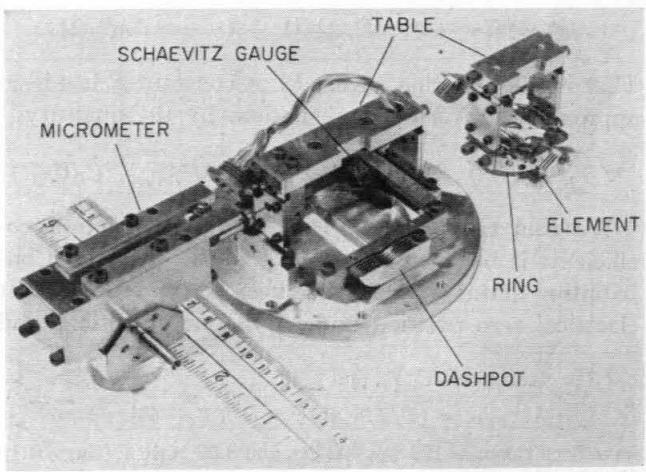

FIG. 3. Separated view of the floating element.

that there was a critical discharge rate, which did not appear to depend on tunnel pressure. For smaller rates than the critical value the airjets had a negligible effect on the distribution of surface friction, while for larger rates the effect was large and did not change appreciably with a further increase in the strength of the disturbance. At $M = 2.0$, the critical decrement in displacement-thickness Reynolds Number was about 10 for values of $u_1\delta^*/\nu_1$ between 700 and 2,000 at the station of the jets. At $M = 4.5$, the boundary-layer transition was less sensitive to discharge rate, and the critical decrement in $u_1\delta^*/\nu_1$ was about 25 for initial values between 3,000 and 5,000.

Friction Measurements

(1) *Local Friction*

The direct friction measurements of the present research are shown in Figs. 5–14. Both the ordinate τ_w/q and the abscissa u_1x/ν_1 have been deduced in an unambiguous way from measured physical quantities. In particular, the static pressure in the balance chambers was used in all cases to determine the local free-stream Mach Number, temperature, velocity, and density. For this calculation the fluid was assumed to be a perfect gas expanding isentropically from the tunnel reservoir with $\gamma = 1.400$, and the Sutherland equation† was used to relate temperature and viscosity.

Two corrections, always amounting together to less than 2 per cent in the shear, have been applied to the data of the figures. First, streamwise pressure forces, caused by small local pressure variations in the element gaps, have been compensated for on the basis of a channel calibration discussed in reference 13. Second, the turbulent friction data, which are relatively sensitive to variations in Mach Number, have been corrected to the nominal Mach Numbers of the figures by means of the approximate relationship

$$(\partial C_f/\partial M)_R = -m^2 C_f/M$$

where

$$m^2 = [(\gamma - 1)\, M^2/2]/[1 + (\gamma - 1)\, M^2/2]$$

That is, the function $C_f(M, R)$ at constant R has been approximated, for this calculation, by the quantity

$$\sqrt{T_1/T_0}\; C_f(0, R) = [1 + (\gamma - 1)M^2/2]^{-1/2} C_f(0, R)$$

Random error in the local turbulent friction coefficients is believed to be less than 2 per cent. Contributing to this error are the uncertainty in the element electrical zero position under dynamic conditions and the uncertainty in both the element static calibration and the micrometer calibration. In addition, the friction measurements at large Mach Numbers required the accurate measurement of tunnel static pressures of the order of 2 to 10 mm. Hg absolute. Both the pressure and the zero position are, of course, relatively more uncertain at low Reynolds Numbers. It was possible, during the profile surveys mentioned below, to repeat some of the shear measurements at the first and second stations. These data are shown as flagged points in Figs. 5–14, and in general indicate excellent reproducibility. The only systematic error that is believed to be important arises because flow over the clearance gaps may contribute to the force on the element; this error probably does not exceed 3 per cent.[13]

(2) *Mean Friction*

The execution of boundary-layer research with impact-probe instrumentation will not be discussed at greater length than is necessary to establish the approximations that are usual in an analysis of the data. It should be noted, however, that the experience of many investigators has shown that an impact probe in a boundary layer is an instrument subject to several sources of error. The presence of the probe may influence the development of the original boundary layer through upstream propagation of pressure disturbances, especially in the case of laminar flow. The existence of a velocity gradient and the proximity of a wall will lead to distortion of the flow pattern around the probe. On the other hand, the use of small probes, in an effort to minimize the problems already mentioned, may introduce new errors associated with viscous dissipation near the probe nose. Finally, the effect of velocity and density fluctuations on the pressure indicated by the probe may not be negligible.

In the present experiments the quantity sought is the momentum thickness, defined by

$$\theta = \int_0^\delta \frac{\rho}{\rho_1}\frac{u}{u_1}\left(1 - \frac{u}{u_1}\right) dy \qquad (1)$$

Fig. 15 shows the variation with y of the integrand in this expression for two typical boundary-layer profiles at a Mach Number of 4.5. The quantity directly measured was, of course, the impact pressure; the static pressure was assumed to correspond to isentropic expansion from the tunnel reservoir with $\gamma = 1.400$ and was taken to be constant through the boundary layer. The latter assumption was in each instance confirmed by measurement of surface pressure near the probe station. From these pressure data the local Mach Number in the boundary layer follows.

The stagnation temperature in the boundary layer has been assumed constant at the value in the tunnel reservoir. The local static temperature, density, velocity of sound, and fluid velocity were obtained from the

† The parameters C, T_r, and μ_r in

$$\mu/\mu_r = (T/T_r)^{3/2}[(T_r + C)/(T + C)]$$

have been taken as 192°R., 492°R., and 3.59×10^{-7} (slugs/ft.^{3})-(ft./sec.)(ft.), respectively.

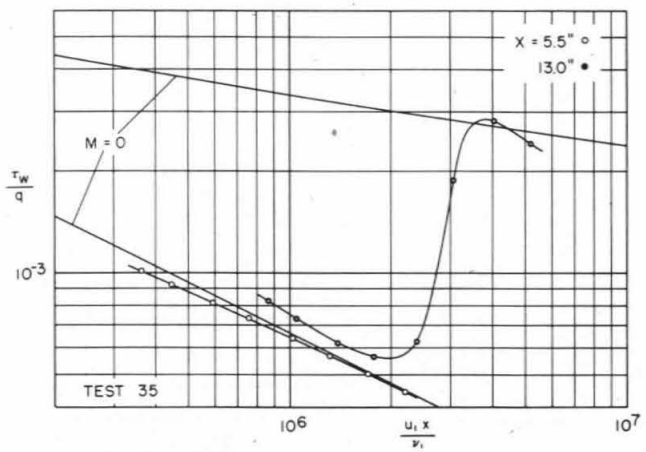

FIG. 5. Local friction, natural transition, $M = 1.97$.

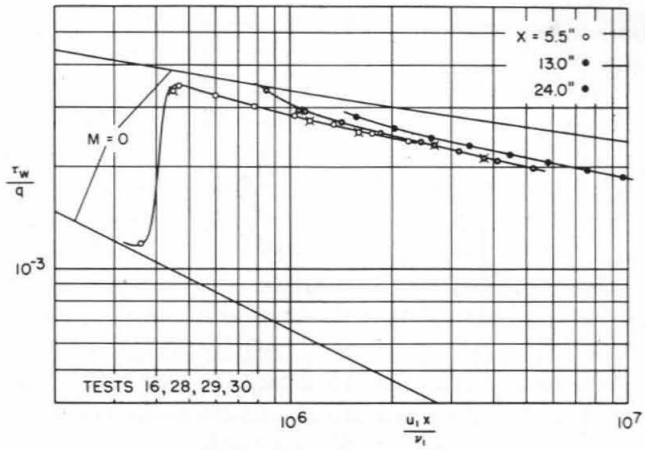

FIG. 6. Local friction, fence trip, $M = 1.97$.

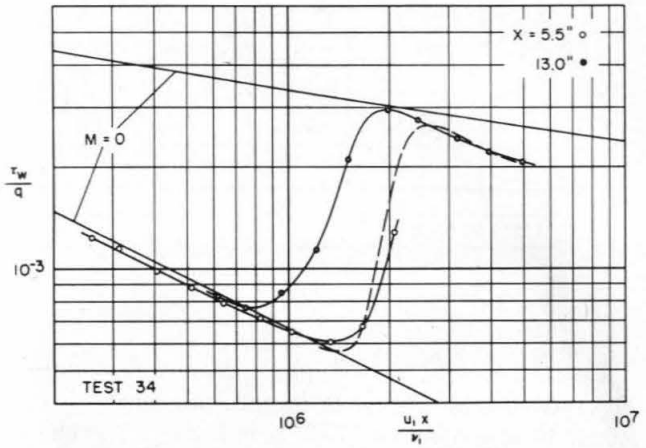

FIG. 7. Local friction, natural transition, $M = 2.57$.

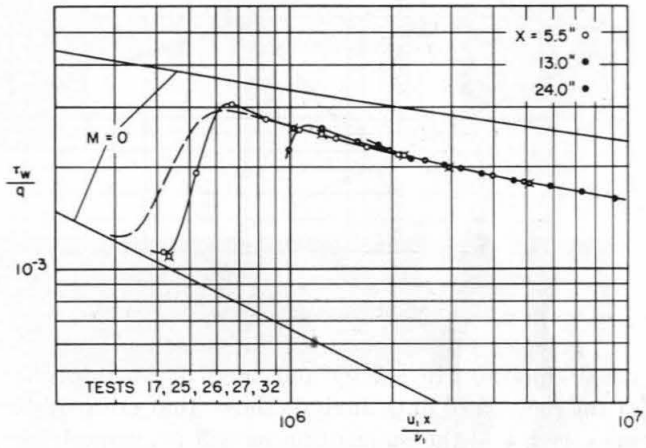

FIG. 8. Local friction, fence trip, $M = 2.57$.

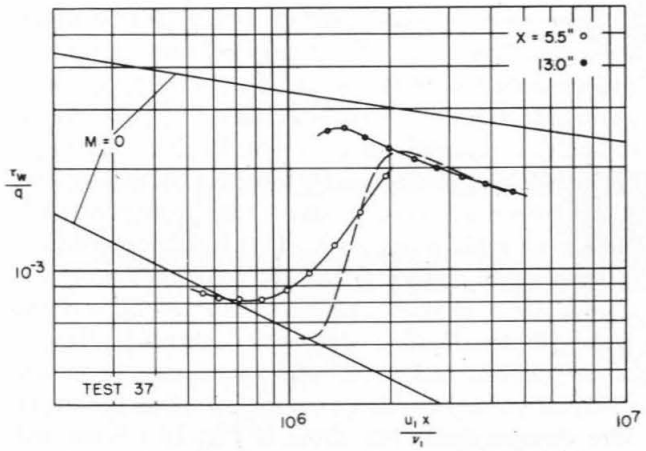

FIG. 9. Local friction, natural transition, $M = 3.70$.

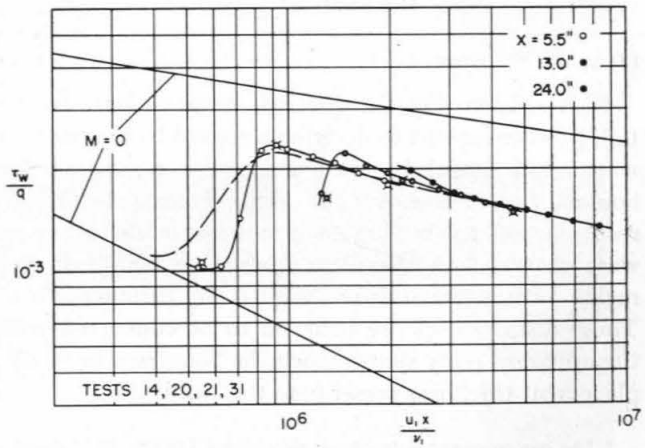

FIG. 10. Local friction, fence trip, $M = 3.70$.

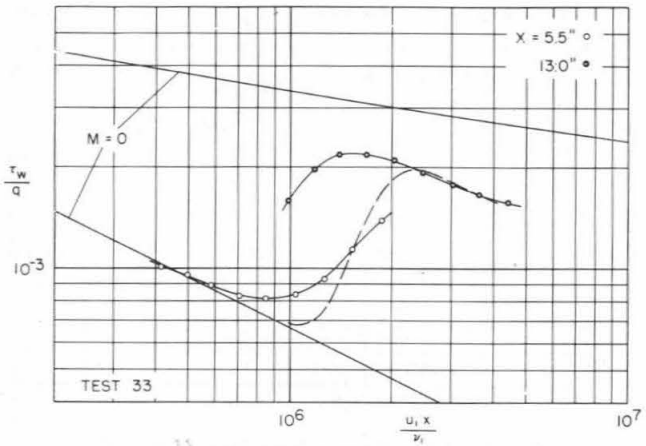

FIG. 11. Local friction, natural transition, $M = 4.54$.

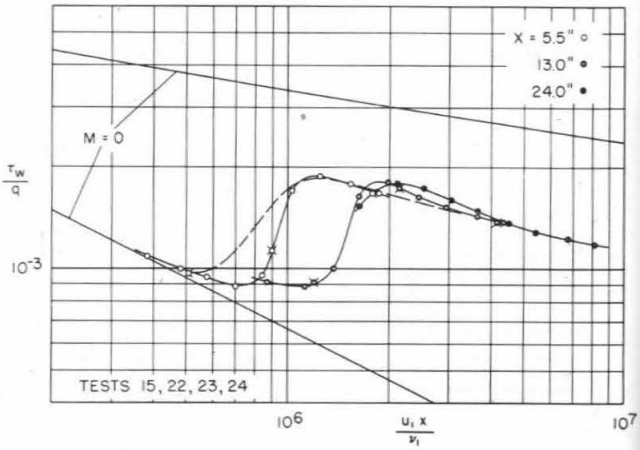

FIG. 12. Local friction, fence trip, $M = 4.54$.

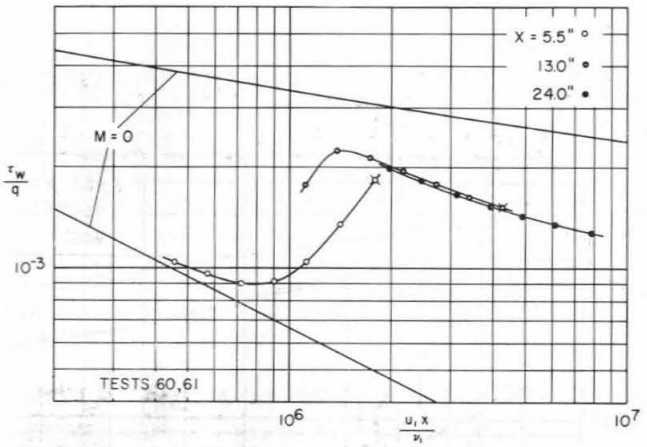

FIG. 13. Local friction, sand trip, $M = 4.54$.

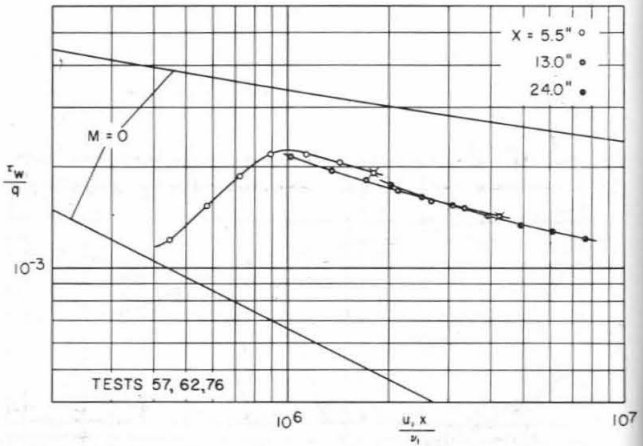

FIG. 14. Local friction, air-jet trip, $M = 4.54$.

usual equations of energy and state.† An inspection of the method of data analysis shows that errors in the velocity u and the momentum ρu will be, respectively, in the same and opposite direction as the error in the local stagnation temperature and will be of half the magnitude. Although the calculation of the integrand in Eq. (1) thus involves a cumulative error at a given point, it seems unlikely that the net error in θ from this source might be larger than the probable uncertainty of a few per cent in the stagnation temperature which is typical for most of the boundary layer.

(3) *Static Pressure*

Before discussing the friction measurements in detail, it is convenient to describe a second technique that was found useful in establishing the nature of the boundary-layer flow over the plate. During the present research, relatively large static-pressure disturbances were observed on the plate surface, especially in the region of transition from laminar to turbulent flow. These disturbances are believed to be connected with the apparent body shape which the boundary-layer displacement thickness presents to the airflow.

† The gas constant $\Re$ has been taken as 1,716 (lb./ft.²)/(slug/-ft.³)(°R.) in the state equation $p = \rho \Re T$.

Figs. 16 and 17 show typical pressure distributions observed during the friction measurements of Figs. 9 and 10 at a nominal Mach Number of 3.7. The expansion downstream of the leading edge and the compression in the transition region are conspicuous when the observed pressures are compared to the empty test-section pressure distribution.

(4) *Transition*

The region of transition from laminar to turbulent flow may be identified by a minimum and a maximum in the curve of local shearing stress plotted against Reynolds Number. The transition is not in general a unique function of the Reynolds Number for the experiments reported here, and this fact increases the difficulty in determining the shear distribution from observations at three points. However, the strong correlation observed between shear and pressure distributions is useful in interpolating between measured values of the friction coefficient at a given stagnation pressure.

Figs. 18–24 show, for the tests with natural transition and with the leading-edge fence, Reynolds Numbers of the minima and maxima in the shear and pressure distributions as obtained from Figs. 5–12 and from pressure measurements like those of Fig. 16. Some judgment has, of course, been exercised in estimating the

Reynolds Numbers for the pressure extrema, since the data are not always adequate to the demands imposed. Furthermore, for technical reasons the pressure measurements were made approximately 3 in. from the tunnel plane of symmetry, and it is not certain that the boundary-layer flow was accurately two-dimensional. In spite of these defects in the pressure data, it appears that the minimum in the static-pressure distribution corresponds closely in all cases to the position of maximum rate of change of the local friction coefficient. It should be remembered that both the friction and pressure measurements in the region of transition represent the response of a highly damped instrument to a quantity that is fluctuating rapidly with time and, therefore, that the present experience with transition may be peculiar to the particular wind tunnel and instrumentation involved.

Several other features of Figs. 18–24 are of special interest. The Reynolds Number per inch, R', is proportional to the tunnel stagnation pressure, and the movement of the natural transition toward smaller values of x but toward larger values of u_1x/ν_1 with increasing tunnel pressure is evident in the coordinate system of the figures. On the other hand, the fence tripping device apparently has the property at high stagnation pressures of causing transition to occur at a fixed Reynolds Number increment from the leading edge. It is therefore possible that the tendency of the corresponding local-friction measurements to define a single curve in the turbulent flow regime is not accidental (see, for example, Fig. 8, where the measurements are relatively insensitive to the presence of local pressure gradients).

At low values of tunnel stagnation pressure, however, the effect of the fence is entirely different. The large

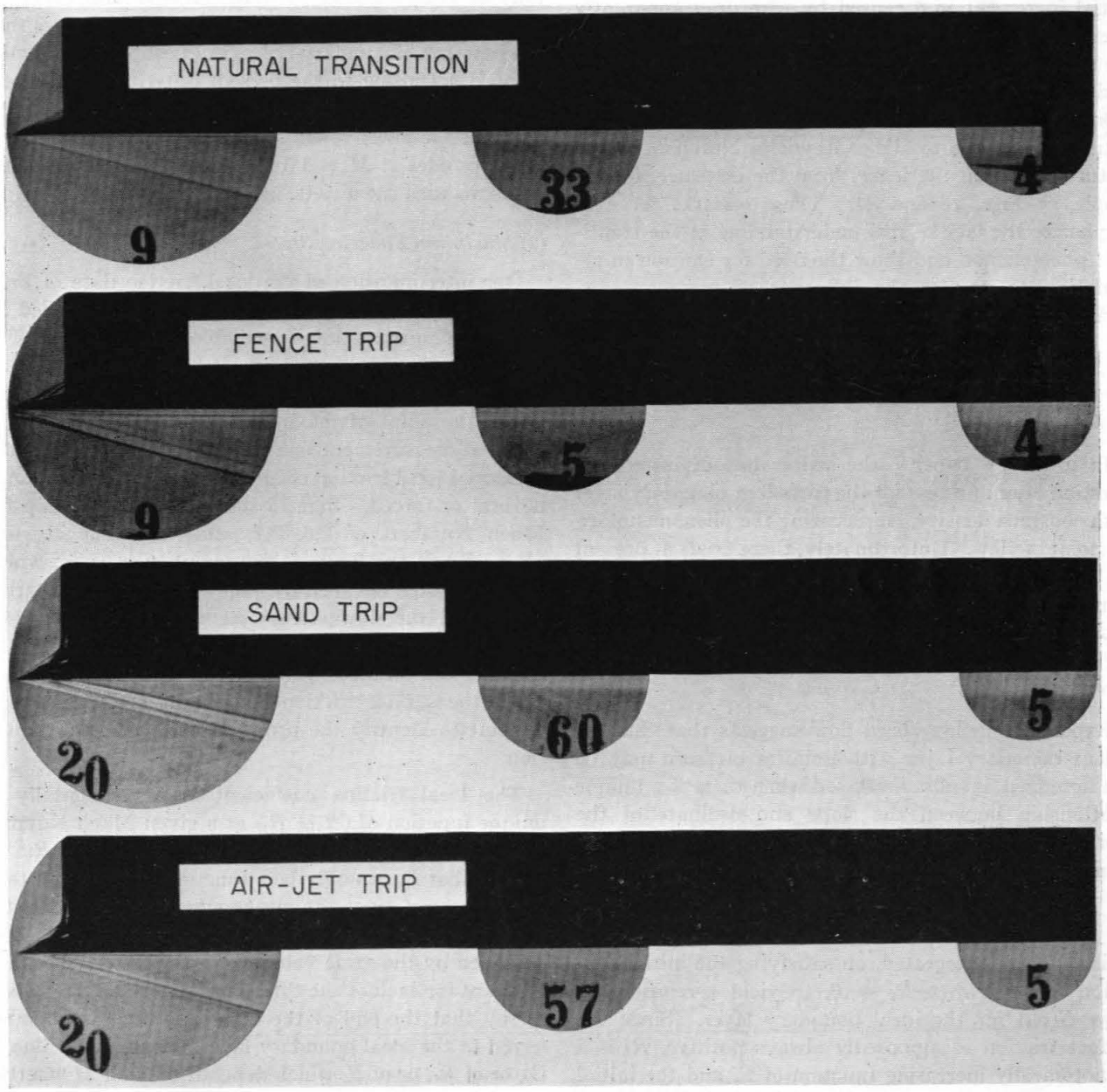

FIG. 4. Schlieren photographs of the boundary layer at $M = 4.5$, $R' = 130{,}000$ per in.

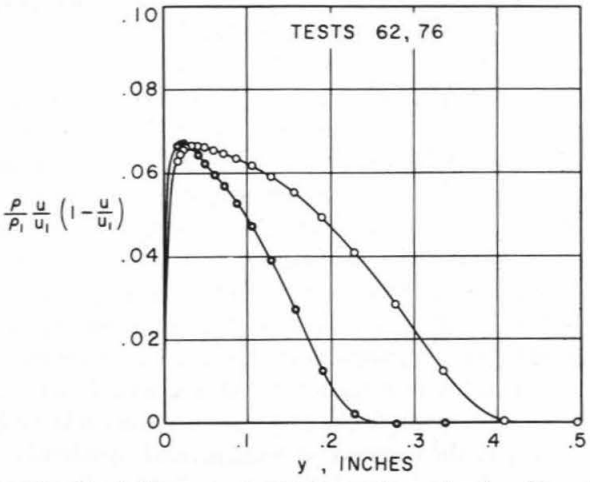

FIG. 15. Typical momentum-thickness determination, $M = 4.5$.

initial increment in θ caused by wire drag apparently does not strongly influence the slope of the velocity profile at the wall upstream of actual transition, as may be verified by a comparison of Figs. 11 and 12. Furthermore, at the lowest tunnel pressures, the transition may actually be moved to higher Reynolds Numbers by the disturbance from the fence, from the evidence, for example, of Figs. 23 and 24. These remarks serve to emphasize the lack of real understanding of the transition phenomenon and show the need for caution in attempting to predict the influence of upstream disturbances.

INTERPRETATION

(1) *Uniqueness*

In a survey paper,[15] the writer has discussed the question of uniqueness for the turbulent boundary layer with constant density, emphasizing the phenomenological point of view. Unfortunately, there exists at present no adequate basis for a generalization of this study to compressible flows. The present discussion will therefore depend entirely on experimental information in attempting to determine the properties of the ideal boundary layer.

Experience in low-speed flow suggests that the turbulent boundary layer with uniform pressure may be characterized as fully developed when there is a unique relationship between the slope and ordinate of the momentum-thickness distribution $\theta(x)$. That is, the assumption of uniqueness implies a function

$$C_f = 2(dR_\theta/dR) = g(R_\theta) \qquad (2)$$

which may be integrated, on satisfying the initial condition $R = 0$ when $R_\theta = 0$, to yield a relationship $R = G(R_\theta)$ for the ideal boundary layer. Since the surface friction is supposedly always positive, R_θ is a monotonically increasing function of R, and the initial condition $R = R_\theta = 0$ can always be satisfied.

However, the integration can be carried out, and an exact definition of R achieved, only if the function g of Eq. (2) is known for all positive values of R_θ. The function in question being defined experimentally, it is clear that any corresponding definition of R is not itself unique and can be valid only in an asymptotic sense. In other words, various experimental determinations of R become equivalent only when R_θ is large compared with values below which the turbulent boundary layer is not observed and is therefore undefined. It also follows, when considering various measurements of turbulent friction, that discrepancies in the final corrected data may not mean that one or another series of measurements is in error but only that they have been differently interpreted.

Fig. 25 shows the relationship between τ_w/q and $u_1\theta/\nu_1$ at various Mach Numbers, as determined experimentally at JPL, together with the corresponding curve for zero Mach Number from reference 15. It appears that the supersonic boundary layers in question are fully developed according to the present criterion, except perhaps for the points that are farthest to the left in the figure at the lower Mach Numbers. In particular, two of the profiles at $M = 4.5$ were obtained with the fence trip, two with the airjets, and one with the sand strip.

(2) *Maximum Shearing Stress*

One interpretation of the local friction data of Figs. 5–12 is suggested by the fact that relatively detailed information on transition is available in Figs. 18–24. For the measurements in question, it has been observed by the writer that the increment in Reynolds Number between the point of maximum shearing stress and the point of measurement is a well-defined function of the measured local friction coefficient, whether transition is natural or forced. Fig. 26 shows this relationship for Mach Numbers of 2.6, 3.7, and 4.5. The abscissa $(R - R_t)$ in the figure is the quantity $u_1\Delta x/\nu_1$, where Δx is measured between the point of maximum shearing stress and the downstream element station for each operating condition. Data at a Mach Number of 2.0 are omitted because small local pressure gradients affect the surface friction and simultaneously make it difficult to identify the pressure disturbance at transition.

The local friction coefficient is experimentally a unique function of $(R - R_t)$ at a given Mach Number and also by assumption a unique function of R. It follows that R_t can only be a function of R for constant M. However, since the measurements at different stations at a fixed value of tunnel pressure should be characterized by the same value of R_t, the latter must be a constant for each of the three curves of Fig. 26. This is to say that the end of the transition region, when referred to the ideal boundary layer, occurs at a value of C_f, or of R_θ, or of R, which depends only on M whether transition is stimulated or not.

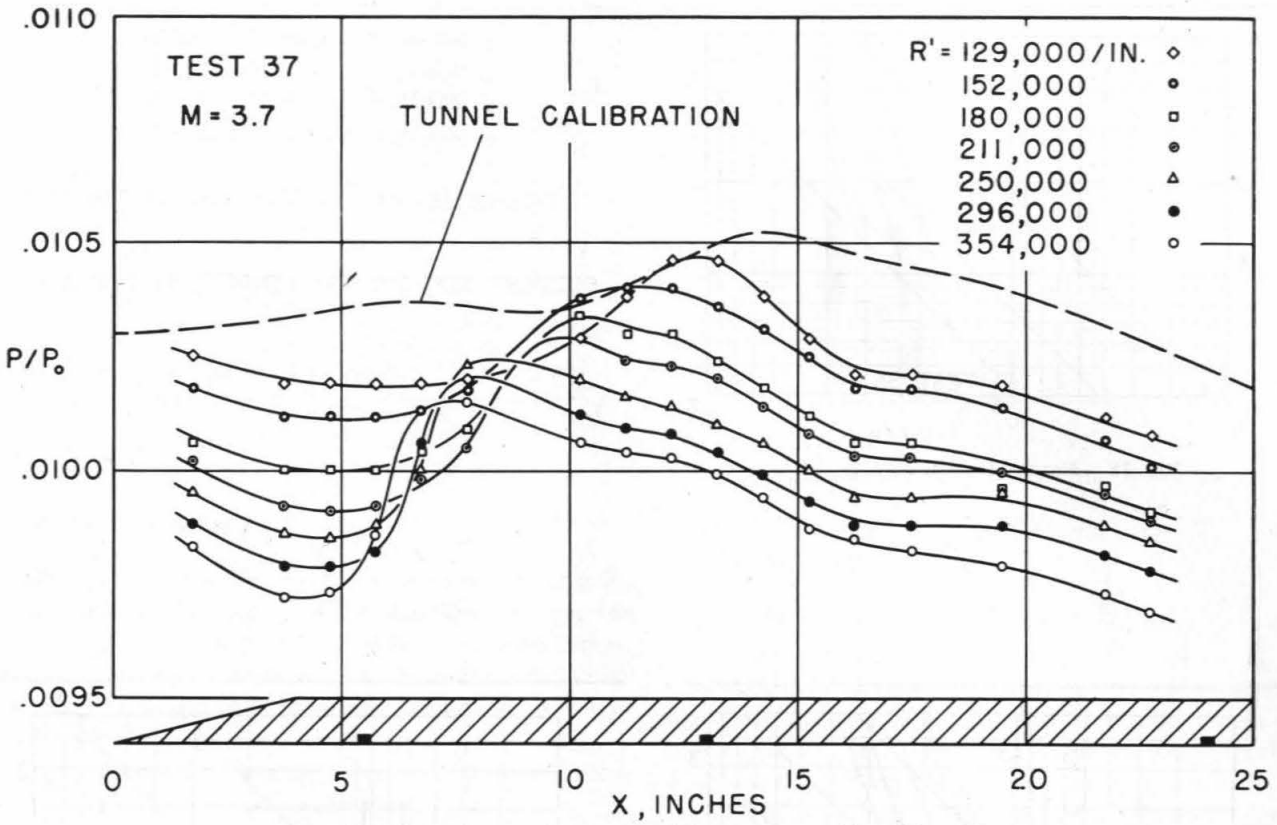

FIG. 16. Static pressure distribution with natural transition, $M = 3.7$.

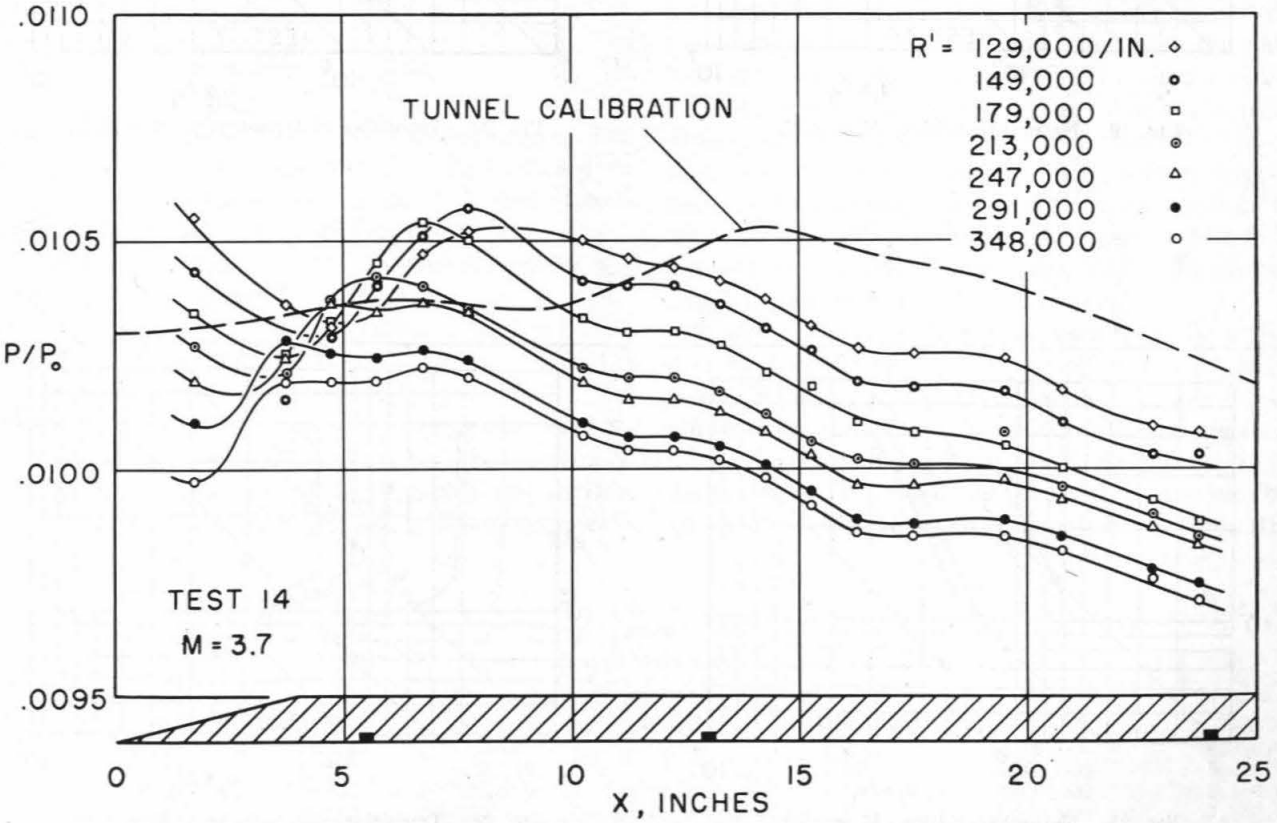

FIG. 17. Static pressure distribution with fence trip, $M = 3.7$.

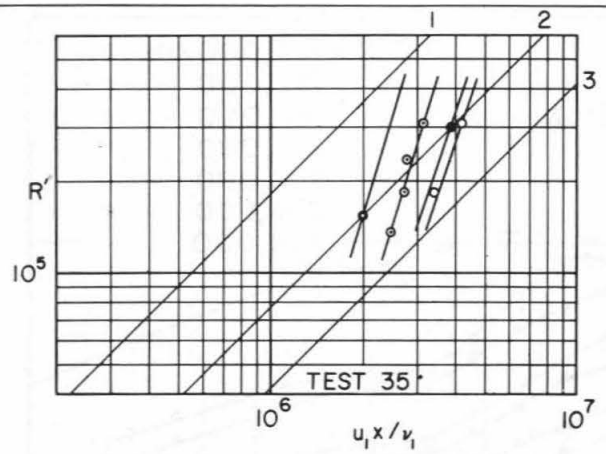

FIG. 18. Natural transition, $M = 1.97$.

- MINIMUM SHEARING STRESS
- MINIMUM STATIC PRESSURE
- MAXIMUM SHEARING STRESS
- MAXIMUM STATIC PRESSURE

FIGURES 18 - 24 OBSERVATIONS OF TRANSITION

ELEMENT STATIONS ARE DENOTED BY 1, 2, 3

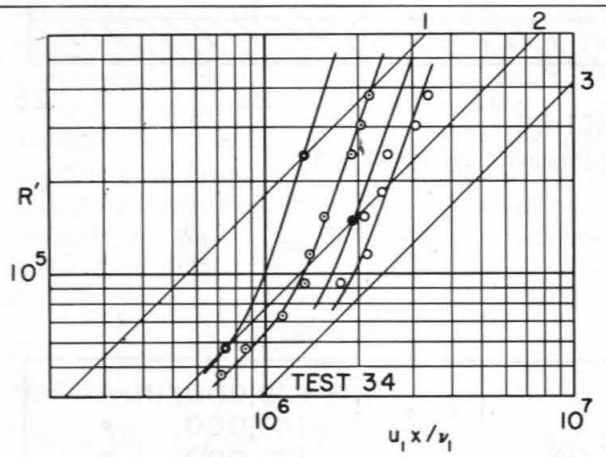

FIG. 19. Natural transition, $M = 2.57$.

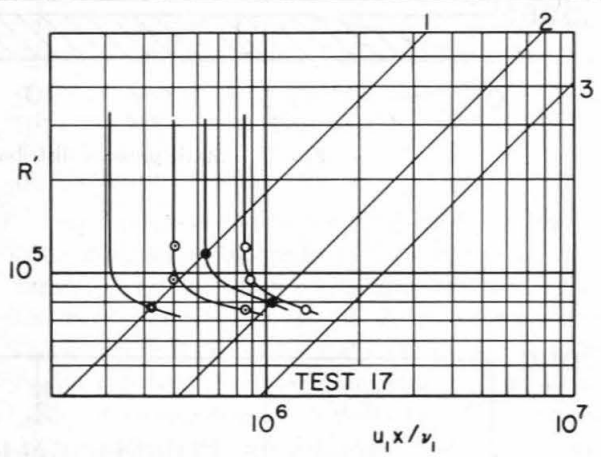

FIG. 20. Transition with fence trip, $M = 2.57$.

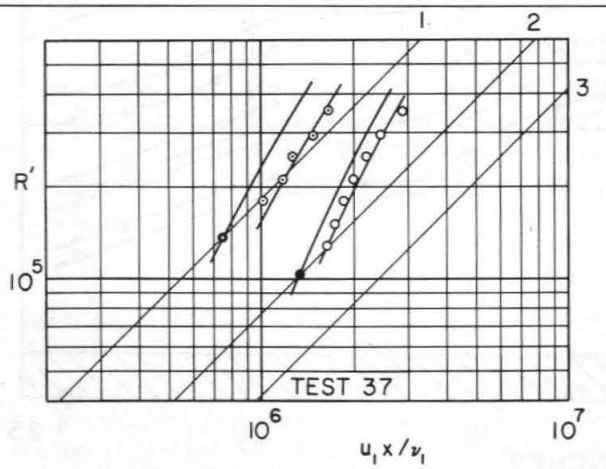

FIG. 21. Natural transition, $M = 3.70$.

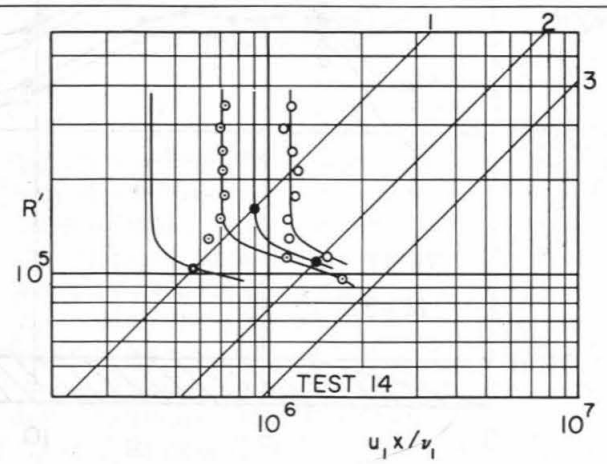

FIG. 22. Transition with fence trip, $M = 3.70$.

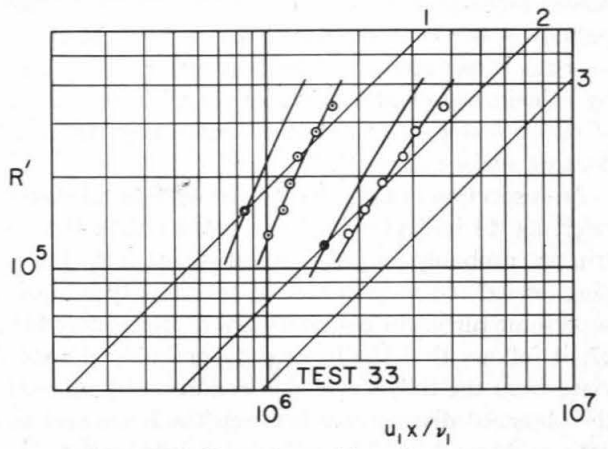

FIG. 23. Natural transition, $M = 4.54$.

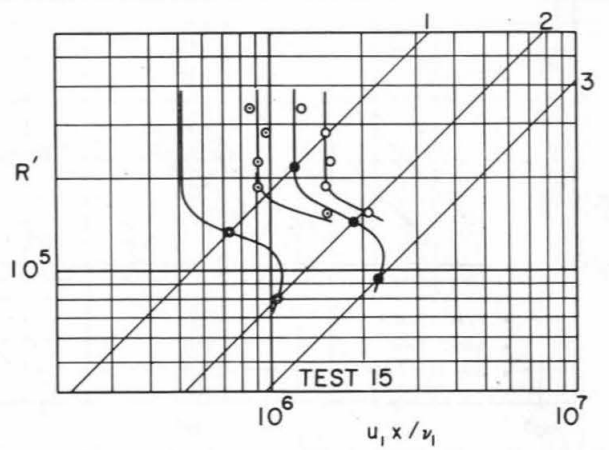

FIG. 24. Transition with fence trip, $M = 4.54$.

(3) *Momentum Balance*

The argument of the preceding section is clearly incomplete. Neither the question of uniqueness nor the question of momentum balance can be resolved experimentally without reference to momentum-thickness measurements, and these have not been cited in developing Fig. 26.

The momentum-integral equation for two-dimensional flow without pressure gradient is

$$C_f = \tau_w/q = 2(d\theta/dx) \tag{3}$$

where the measured quantities $2d\theta/dx$ and τ_w/q represent, respectively, the rate of momentum loss in the fluid and the drag force on the surface. For the experiments with the fence trip, Eq. (3) may be integrated in the form

$$\theta = \theta_0 + \int_0^x \frac{\tau_w}{2q}\, dx \tag{4}$$

where θ_0 is the contribution of the tripping device. For example, if the drag coefficient of a cylinder based on projected area is 1.2 for the range of M and R considered here, then[14] $\theta_0 = 0.0034$ in.

Multiplying Eq. (4) by the Reynolds Number per inch, R', there is obtained

$$R_\theta = R'\theta_0 + \int_0^{u_1 x/\nu_1} \frac{\tau_w}{2q}\, dR'x \tag{5}$$

This expression is to be applied to measurements of R_θ with x fixed and R' variable. However, the behavior of the transition curves in Figs. 20, 22, and 24 implies that τ_w/q in the laminar, transition, and turbulent regimes is a function of $u_1 x/\nu_1$ only, at least for large R'. Thus Eq. (5) becomes

$$R_{\theta_2} - R_{\theta_1} = \int_{R'_1 x}^{R'_2 x} \left(\frac{\tau_w}{2q} + \frac{\theta_0}{x}\right) dR'x \tag{6}$$

It is evident at once that the measurements with the fence trip must violate the principle of uniqueness expressed by Eq. (2). If Eq. (6) is correct, it follows that R_θ cannot be a unique function of τ_w/q when R' is variable and θ_0 is different from zero. It also follows that Fig. 26 should be viewed with suspicion, since the evidence is against the proposition that a unique value of R_θ can be associated with each point in the figure.

Integration of Eq. (6) may be carried out conveniently in Fig. 26, on replacing the variable of integration $R'x$ by the equivalent quantity $(R - R_t)$. Table 1 lists some observed values of $(R_{\theta_2} - R_{\theta_1})$, together with the corresponding quantities computed from the right-hand side of Eq. (6) using $\theta_0 = 0.0034$ in. and $x = 21.5$ in. The general agreement in the table confirms the supposition that τ_w/q is a function of $(R_\theta - R'\theta_0)$ rather than of R_θ for the experiments with the fence tripping device. In other words, a residual disturbance from the fence is detectable, at least in part, as an additive increment in R_θ, and the hypothesis of uniqueness is therefore not supported by these data.

Whether this conclusion is important in the present context depends on whether the effect can be distinguished in Fig. 25. In particular, Eq. (6) may be considered merely as a formula for experimental continuation of the direct measurements of R_θ given in the figure, the continuation being consistent with momentum balance without assuming uniqueness. In this sense, Eq.

TABLE 1

Investigation of Momentum Balance

M	Tests	Trip	$(R_{\theta_2} - R_{\theta_1})$ Eq. (6)	$(R_{\theta_2} - R_{\theta_1})$ Eq. (5)	$(R_{\theta_2} - R_{\theta_1})$ Observed	$(R_2 - R_1)$ Eq. (7)	$(R_2 - R_1)$ Fig. 25
2.6	27, 26	Fence	3,540	...	3,600	4,200,000	4,300,000
3.7	20, 19	Fence	3,310	...	3,460	4,650,000	5,050,000
4.5	23, 22	Fence	2,960	...	3,120	4,600,000	5,150,000
4.5	76, 62	Air jet	...	2,440	2,340	3,400,000	3,850,000

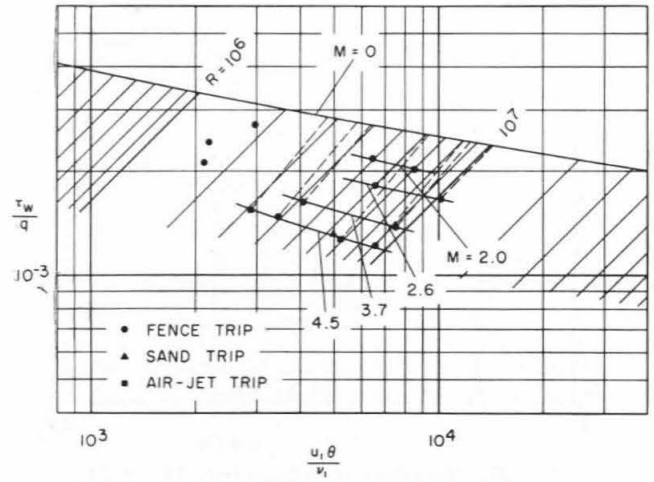

FIG. 25. Determination of ideal Reynolds Number.

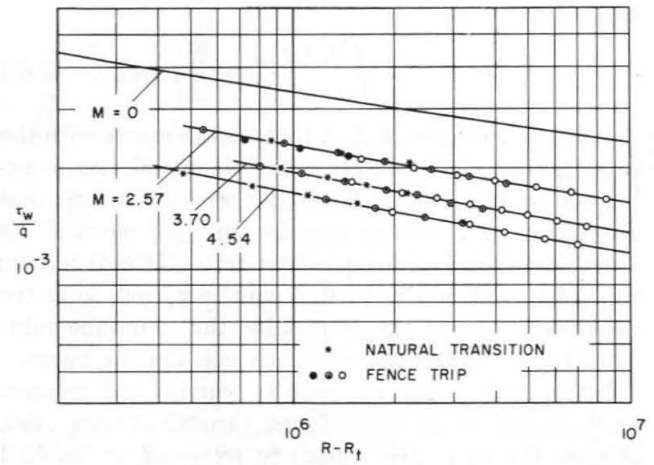

FIG. 26. Equivalence of natural and forced transition.

(6) allows the data of Fig. 26 to be transferred to the coordinate system of Fig. 25, with the result shown in Fig. 27.

Finally, a joint test of the hypotheses of uniqueness and momentum balance can be carried out by direct calculation from Eq. (5). Choosing a value for R' of 290,000 per in., local friction distributions can be estimated as shown by the dashed lines in Figs. 7–12. The relationship between R_θ and τ_w/q obtained by integration of Eq. (5) is found in each case to j oin smoothly onto the appropriate experimental curve, as shown in Fig. 27.

For the fence trip, the computed values of R_θ at the most downstream station are found to be a few per cent smaller than values obtained by experimental continuation—i.e., than values measured directly. This discrepancy, while not important in Fig. 27, should be compared to the result of a less equivocal investigation of momentum balance at a Mach Number of 4.5 with the airjet trip. The relevant profile data at two stations at the same tunnel pressure have already been presented in Fig. 15. Table 1 lists the experimentally observed increment $(R_{\theta_2} - R_{\theta_1})$, together with the increment calculated from Eq. (5) with $\theta_0 = 0$; the observed increase in R_θ between the two probe stations is perhaps 4 per cent smaller than the integral of $\tau_w/2q$ over the same interval. The discrepancy of 4 per cent, by coincidence or otherwise, agrees with an estimate[13] of the probable effect of the clearance gaps around the floating surface element.

An inspection of the velocity profile data tabulated in reference 14 indicates that the profiles with the airjet trip are probably free of residual effects from the tripping device and may in fact be taken as typical of the supersonic turbulent boundary layer. Returning to Fig. 27, it follows that the fence data probably do not deviate from the fully developed condition by more than the observed discrepancy between the fence and airjet data at $M = 4.5$. The collected points in Fig. 27 are therefore certified as representing the fully developed turbulent boundary layer, within the degree of accuracy implied both by the comparison just given and by the estimate already made of possible systematic error in measurement of shearing stress.

(4) Reynolds Number

One method of obtaining Reynolds Numbers for the present data requires the supersonic measurements to be compatible with measurements at zero Mach Number and to be internally consistent in terms of the momentum-integral equation, Eq. (3). Given a pair of boundary-layer profiles at the same Mach Number but different Reynolds Numbers, an average local friction coefficient can be defined by

$$C_{f_{\text{avg.}}} = \frac{1}{R_2 - R_1}\int_{R_1}^{R_2} C_f\, dR = 2\,\frac{R_{\theta_2} - R_{\theta_1}}{R_2 - R_1} \qquad (7)$$

It is easily shown that the average coefficient expressed by Eq. (7) is, for practical purposes, identical with that given by

$$C_{f_{\text{avg.}}} = \frac{1}{R_{\theta_2} - R_{\theta_1}}\int_{R_{\theta_1}}^{R_{\theta_2}} C_f\, dR_\theta \qquad (8)$$

when a power law is assumed for the variation of C_f with R_θ within the interval in question—i.e., a straight line in

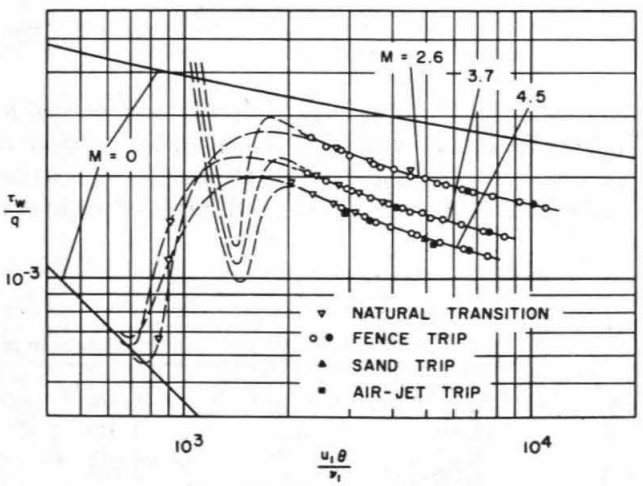

FIG. 27. The ideal boundary layer.

TABLE 2
Tentative Reduction to Ideal Conditions

M	Test	Trip	u_1x/ν_1	R	R_θ	C_f	C_F	C_f/C_{f_i}	C_F/C_{F_i}
2.6	27	Fence	4,840,000	6,080,000	6,600	0.00181	0.00217	0.705	0.715
2.6	26	Fence	8,320,000	10,260,000	10,200	0.00166	0.00199	0.700	0.710
3.7	20	Fence	3,540,000	3,980,000	4,100	0.00162	0.00206	0.595	0.635
3.7	19	Fence	7,250,000	8,630,000	7,550	0.00138	0.00175	0.570	0.610
4.5	76	Air jet	3,370,000	2,810,000	2,900	0.00155	0.00206	0.535	0.600
4.5	23	Fence	3,520,000	3,570,000	3,470	0.00148	0.00194	0.530	0.590
4.5	62	Air jet	6,910,000	6,200,000	5,240	0.00125	0.00169	0.495	0.560
4.5	22	Fence	6,830,000	8,170,000	6,590	0.00122	0.00161	0.500	0.560

Fig. 25. Taking $C_f = AR_\theta^{-1/n}$ in Eq. (8), then

$$C_{f_{\text{avg.}}} = \frac{(R_{\theta_2}C_{f_2} - R_{\theta_1}C_{f_1})/(R_{\theta_2} - R_{\theta_1})}{1 - \ln(C_{f_1}/C_{f_2})/\ln(R_{\theta_2}/R_{\theta_1})} \tag{9}$$

Values of $(R_2 - R_1)$ calculated from Eq. (7), using the average coefficient from Eq. (9), are listed in Table 1. As has been pointed out, the second entry for $M = 4.5$ involves two profiles at different plate stations at the same tunnel pressure, with the airjet trip, and the remaining data involve two profiles at different pressures at the same station, with the fence trip.

Consulting Fig. 25, a straight line that slopes up and to the right at 45° is a line on which $C_f(M)/C_f(0)$ and $R_\theta(M)/R_\theta(0)$ are equal; it may be assumed initially to be also a line of constant Reynolds Number. Absolute values of R follow on integrating Eq. (2) in an asymptotic sense already defined; the result[15] for $M = 0$ is shown in Fig. 25. Values of R for the ideal supersonic boundary layer are conveniently determined by interpolation, and the increment $(R_2 - R_1)$ thus derived for the various paired profiles is given in Table 1.

The second method for calculating $(R_2 - R_1)$ may be reconciled with the first by assuming that lines of constant R in Fig. 25 have a slope which is not 45° but is at least independent of Reynolds Number in the range being considered. The problem is then reduced to one of determining the proper slope so that the intercepts on the curve $M = 0$ are separated by the desired increment in R. Such lines are shown in the figure; they correspond to the values of R, and of $C_f/C_{f_i} = C_f(M)/C_f(0)$ and $C_F/C_{F_i} = R_\theta(M)/R_\theta(0)$ at constant R, which are listed in Table 2. The result of the calculation is relatively insensitive to errors in measurement of either shearing stress or momentum thickness. In particular, it is easily shown that the value of $(C_f/C_{f_i})/(C_F/C_{F_i})$ for a given pair of profiles would be unaffected if the measured values of τ_w/q or R_θ were corrected by a small fixed percentage to account for a suspected experimental error. It follows that the development leading to Table 2 does not depend significantly on the question of uniqueness raised in the preceding sections.

It should be pointed out that difficulty in defining an ideal Reynolds Number is not necessarily material in practical calculations of flat-plate drag. For example, the original values of u_1x/ν_1 for a typical curve in Fig. 27 can obviously be recovered by integrating Eq. (2),

$$\frac{u_1x}{\nu_1} = 2\int_{R'\theta_0}^{R_\theta} \frac{dR_\theta}{g(R_\theta)} \tag{10}$$

with $g(R_\theta) = C_f(R_\theta)$ defined experimentally. A corresponding calculation can be carried out for any plate flow for which the transition curve in Fig. 27 is known or can be estimated. In practice, it may be convenient to begin with the coordinate system $C_f(R)$ of Figs. 5–14, taking the laminar flow as an initial state and assuming a distribution of local friction for the first half of the transition region. The function $R_\theta(R)$ then follows on integrating the conventional expression for momentum balance, Eq. (5). The result of the integration can be transferred to the coordinate system $C_f(R_\theta)$ of Fig. 27 and can be suitably connected to the curve describing the known final state of the boundary layer. Eq. (10) may then be used to continue the calculation indefinitely.

(5) *The Ideal Boundary Layer*

The uniqueness criterion expressed by Eq. (2) is clearly a vital concept in any evaluation of experimental data obtained in turbulent boundary layers. For low-speed flow, this concept leads immediately to an intuitive definition of ideal Reynolds Number and eventually to a quantitative definition based on certain characteristic properties of the mean-velocity profile. According to the evidence considered in reference 15, the development of a turbulent boundary layer with constant density may be divided roughly into four regions:

(1) For momentum-thickness Reynolds Numbers R_θ greater than about 5,000, the turbulent mean-velocity profile follows certain well-defined laws of similarity. The contribution of the sublayer to the streamwise flow of mass or momentum is negligible.

(2) For R_θ between 2,000 and 5,000, the similarity laws apply, but the sublayer flow should be taken into account.

(3) For R_θ between 500 and 2,000, the mean-velocity profile is probably unique, but the similarity laws are not strictly valid.

(4) For R_θ less than about 500, fully turbulent flow is rarely observed.

In the region (1), the relationship between τ_w/q and R_θ has a simple analytic form involving four dimensionless parameters. If this expression is arbitrarily adopted

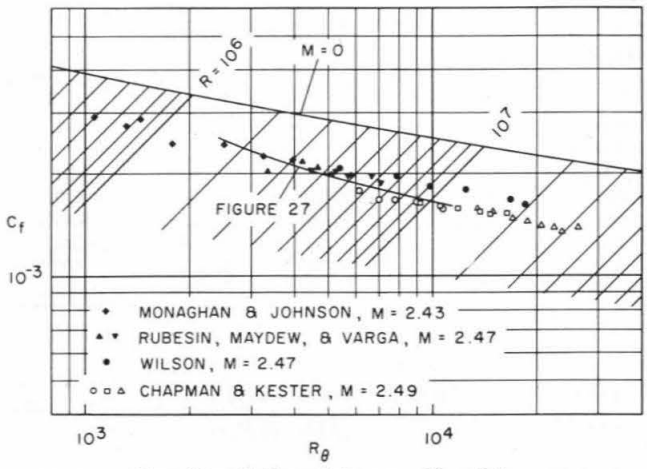

FIG. 28. Collected data at $M = 2.5$.

as the uniqueness relationship of Eq. (2), then the Reynolds Number defined by integration[15] will be valid in an asymptotic sense for large values of R_θ.

As the generalized similarity laws for the compressible mean-velocity profile are unknown, the corresponding definition of Reynolds Number in terms of an asymptotic state is not yet possible. It is therefore necessary to classify as tentative any quantitative results of the present report which are not independent of, or at least insensitive to, the definition of an ideal Reynolds Number. In particular, emphasis should be placed on Fig. 27 rather than on Fig. 26, and more importance should be attached to the values of C_f/C_{f_i} in Table 2 than to the values of C_F/C_{F_i}.

One of the original objectives of the research reported here was to discriminate among several theoretical analyses of the compressible turbulent boundary layer. However, during study of the experimental data it became obvious that the most conspicuous effect of compressibility is to move the various stages of boundary-layer development toward larger values of R_θ. For example, the effect of surface heating at large Mach Numbers is known to be manifested in thickening of the sublayer,[12, 14] so that the final stage of turbulent boundary-layer flow must be reached at progressively larger values of R_θ as M increases. This effect is overlooked in the theoretical literature with one exception.[18]

Finally, it is important to note in Fig. 27 that fully developed turbulent flow was apparently not observed in the JPL experiments for R_θ smaller than about 2,000. In the absence of other evidence, therefore, it is recommended that values of R_θ substantially larger than 2,000 be stipulated for any fundamental future study of friction, heat transfer, or other phenomena in supersonic turbulent boundary layers.

APPENDIX.—COMPARISON WITH OTHER DATA AT $M = 2.5$

For two-dimensional flow over a flat plate, it is readily shown that the complete form of the momentum-integral equation (3) is†

$$\frac{\tau_w}{q} = 2\frac{d\theta}{dx} - (2 - M^2 + \delta^*/\theta)\frac{\theta}{q}\frac{dp}{dx} \qquad (11)$$

It has been found experimentally[14, 19–21] that the value of the profile parameter δ^*/θ is very nearly 4.2 for turbulent flow at Mach Numbers near 2.5, and it follows that the combination $(2 - M^2 + \delta^*/\theta)$ in Eq. (11) is negligibly small. This property of the momentum-integral equation is an important reason for studying experimental data at $M = 2.5$, since the boundary layer should be insensitive to local variations in static pressure.

Profile measurements in turbulent boundary layers at Mach Numbers between 2.4 and 2.5 have been reported by Wilson,[19] by Monaghan and Johnson,[20] and by Rubesin, Maydew, and Varga.[21] In each of these investigations the momentum-thickness distribution $\theta(x)$ on a flat plate was observed for a fixed tunnel condition, and $2d\theta/dx$ can be computed immediately as a function of R_θ. Values calculated by the writer are represented by solid symbols in Fig. 28, and the corresponding curve for $M = 0$ from reference 15 is also shown.

The data derived from profile surveys appear at first glance to define a unique boundary layer. Moreover, the fact that the experimental curves for $M = 0$ and $M = 2.5$ are parallel suggests that $C_f(M)/C_f(0)$ is, in fact, independent of Reynolds Number. The slope and ordinate of the function $R_\theta(R)$ are therefore affected equally and uniformly by compressibility, and a line of constant R has a slope of 45° in Fig. 28.

Values of R obtained by interpolation in Fig. 28 are plotted against u_1x/ν_1, the Reynolds Number measured from the leading edge, in Fig. 29. In each case the ordinate and abscissa differ by a constant that agrees closely with the value chosen in the original paper. This result is not surprising, since each of the original analyses determined an apparent origin by referring the supersonic measurements to flow at $M = 0$ and by assuming the effect of compressibility to be nearly or exactly independent of Reynolds Number.

Chapman and Kester[9] have recently measured directly the friction drag on the cylindrical afterbody of a cone-cylinder model at a Mach Number of 2.5. Small corrections were introduced to compensate for a starting length upstream of the region of measurement, using the fact that $C_F(M)/C_F(0)$ was found experimentally to be independent of Reynolds Number at constant Mach Number. Since the mean and local friction coefficients satisfy a relationship $C_f = d(C_FR)/dR$, where by definition $C_f = \tau_w/q$ and $C_F = D/2\pi rqx$, it is convenient to represent C_F in a limited region by the power law $C_F = AR^{-1/n}$; then $C_f = C_F[1 - (1/n)]$. Assuming that a value of $1/n = 0.17$ is appropriate to the data for $M = 2.5$ in Fig. 8 of reference 9, the meas-

† $\delta^* = \int_0^\delta \left(1 - \frac{\rho}{\rho_1}\frac{u}{u}\right) dy.$

urements in question lie as shown by the open points in Fig. 28. Because R_θ was not measured in these experiments, the data have been plotted against $C_F R/2$, which is supposedly equivalent to R_θ when the latter is suitably defined in cylindrical coordinates. No attempt has been made to correct the original values of C_F for the influence of curvature, although it is clear that any such correction should affect ordinate and abscissa equally in Fig. 28. Values of R obtained by interpolation are found to agree with values given in reference 9 for a length/diameter ratio of 8 and are found to be a few per cent smaller for length/diameter ratios of 13 and 23.

If any conclusion can be drawn from the experience of the several investigators who have measured turbulent friction in supersonic flow, it is that more study of experimental techniques is needed. Fig. 28 in some cases exhibits a serious disagreement between measurements of drag and of momentum loss at a Mach Number of 2.5. The only direct verification of momentum balance known to the writer is the one reported here, which was obtained on a smooth but unpolished surface at $M = 4.5$ with an airjet trip. It is entirely possible that surface roughness may be a factor in causing the disagreement noted in Fig. 28. However, the writer's personal conviction is that too much attention, rather than too little, is probably paid to surface finish in investigations concerned primarily with flow downstream of transition.

Experience at JPL does not suggest an explanation for the discrepancies in Fig. 28. The effects of pressure gradient have already been discounted, and any systematic error in momentum-thickness measurements should be common to all the experiments considered here.

It should be noted in connection with profile surveys that the momentum thickness at large Mach Numbers is highly sensitive to the shape of the velocity profile at the outer edge of the boundary layer. On assuming constant stagnation temperature and static pressure, so that a relationship between ρ and u is known, the maximum value of the integrand in Eq. (1) can be computed as a function of Mach Number. The value in question is 0.250 at $M = 0$, 0.131 at $M = 2.55$, and 0.067 at $M = 4.55$. However, the integrand in Eq. (1) behaves like $[1 - (u/u_1)]$ near the outer edge of the boundary layer. On referring to Fig. 15 for a typical profile, it is clear that a given error in velocity must lead to relatively larger errors in the ordinate, and therefore in θ, as the Mach Number increases. Moreover, if the phenomenon of intermittence observed in low-speed flow persists at supersonic speeds, the velocity deduced from impact by pressure measurements may depend on the nature of the intermittence and on the probe response to a fluctuating signal.

It is also possible that the ambient flow in a typical supersonic wind tunnel deviates sufficiently far from the two-dimensional condition to account for all or part of the inconsistency observed in Fig. 28. The practice

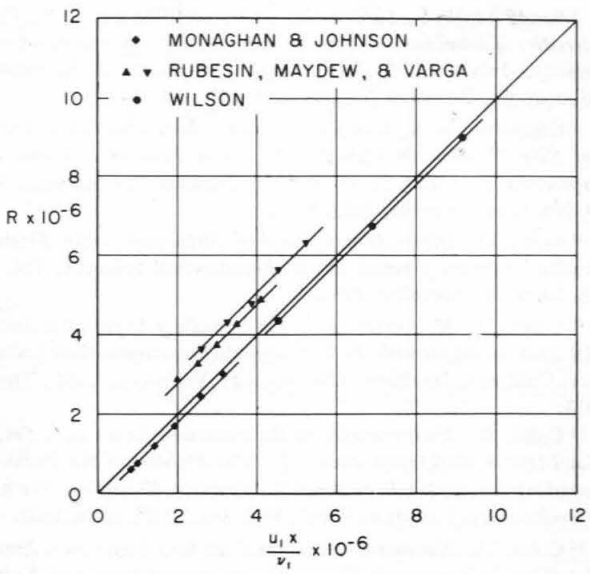

FIG. 29. Comparison of real and ideal Reynolds Numbers.

of making an adjustment in the top and bottom nozzle contours, to account for the presence of a boundary layer on all four tunnel walls, leads inevitably to three-dimensional flow in the test section. The flow is slightly converging in the plan view and slightly diverging in the elevation. The two effects cancel as far as the pressure distribution on the tunnel axis is concerned, yielding there a uniform value of static pressure. In the 20-in. tunnel at JPL, pressure and flow inclination surveys off the nozzle centerline at a Mach Number of 2.6 have definitely established the presence of this peculiarity in the supposedly uniform flow.

REFERENCES

[1] Kempf, G., *Neue Ergebnisse der Widerstandsforschung*, Werft-Reederei-Hafen, Vol. 10, No. 11, pp. 234–239; No. 12, pp. 247–253, 1929.

[2] Schultz-Grunow, F., *Neues Reibungswiderstandsgesetz für glatte Platten*, Luftfahrtforschung, Vol. 17, No. 8, pp. 239–246, August, 1940; translated as *New Frictional Resistance Law for Smooth Plates*, NACA TM No. 986, September, 1941.

[3] Ginsburgh, A. S., *Supersonic Skin Friction Drag Measurements at a Mach Number of 1.72*, United Aircraft Corporation, Project Meteor, Rep. No. UAC-17, February, 1948.

[4] Liepmann, H. W., and Dhawan, S., *Direct Measurements of Local Skin Friction in Low-speed and High-speed Flow*, Proc. First U.S. National Congress of Applied Mechanics, pp. 869–874, Chicago, 1951; see also Dhawan, S., *Direct Measurements of Skin Friction*, Guggenheim Aeronautical Laboratory, California Institute of Technology, Pasadena, Calif., Thesis, 1951, or NACA TN No. 2567, January, 1952.

[5] Hakkinen, R. J., *Measurements of Skin Friction in Turbulent Boundary Layers at Transonic Speeds*, Guggenheim Aeronautical Laboratory, California Institute of Technology, Pasadena, Calif., Thesis, 1953.

[6] Weiler, J. E., and Hartwig, W. H., *The Direct Determination of Local Skin Friction Coefficient*, Defense Research Laboratory, University of Texas, Austin, Tex., Rep. No. DRL-295 (CF-1747), January, 1952.

[7] Eimer, M., *Experimental Skin Friction at Hypersonic Mach Numbers*, Guggenheim Aeronautical Laboratory, California Institute of Technology, Pasadena, Calif., Thesis, 1953.

[8] Bradfield, W. S., DeCoursin, D. G., and Blumer, C. B., *Characteristics of Laminar and Turbulent Boundary Layer at Supersonic Velocity*, Institute of Technology, University of Minnesota, Minneapolis, Research Rep. No. 83, July, 1952.

[9] Chapman, D. R., and Kester, R. H., *Measurements of Turbulent Skin Friction on Cylinders in Axial Flow at Subsonic and Supersonic Velocities*, Journal of the Aeronautical Sciences, Vol. 20, No. 7, pp. 441–448, July, 1953.

[10] Coles, D., *Direct Measurement of Supersonic Skin Friction*, Readers' Forum, Journal of the Aeronautical Sciences, Vol. 19, No. 10, p. 717, October, 1952.

[11] Coles, D., *Measurements in the Boundary Layer on a Smooth Flat Plate in Supersonic Flow*, Guggenheim Aeronautical Laboratory, California Institute of Technology, Pasadena, Calif., Thesis, 1953.

[12] Coles, D., *Measurements in the Boundary Layer on a Smooth Flat Plate in Supersonic Flow. I. The Problem of the Turbulent Boundary Layer*, Jet Propulsion Laboratory, California Institute of Technology, Pasadena, Calif., Rep. No. 20-69, June, 1953.

[13] Coles, D., *Measurements in the Boundary Layer on a Smooth Flat Plate in Supersonic Flow. II. Instrumentation and Experimental Techniques at the Jet Propulsion Laboratory*, Jet Propulsion Laboratory, California Institute of Technology, Pasadena, Calif., Rep. No. 20–70, June, 1953.

[14] Coles, D., *Measurements in the Boundary Layer on a Smooth Flat Plate in Supersonic Flow. III. Measurements in a Flat Plate Boundary Layer at the Jet Propulsion Laboratory*, Jet Propulsion Laboratory, California Institute of Technology, Pasadena, Calif., Rep. No. 20–71, June, 1953.

[15] Coles, D., *The Problem of the Turbulent Boundary Layer*, submitted to the editor, Zeitschrift für angewandte Mathematik und Physik, July, 1953; to be published in 1954.

[16] Schaevitz, H., *The Linear Variable Differential Transformer*, Proc. Society for Experimental Stress Analysis, Vol. 4, No. 2, pp. 79–88, 1947.

[17] Fage, A., and Sargent, R. F., *An Air-injection Method of Fixing Transition from Laminar to Turbulent Flow in a Boundary Layer*, British ARC, R. & M. No. 2106, June, 1944.

[18] Donaldson, C. du P., *Skin Friction and Heat Transfer through Turbulent Boundary Layers for Incompressible and Compressible Flows*, 1952 Heat Transfer and Fluid Mechanics Institute, Los Angeles, pp. 19–35, June, 1952; see also *On the Form of the Turbulent Skin Friction Law and its Extension to Compressible Flows*, NACA TN No. 2692, May, 1952.

[19] Wilson, R. E., *Turbulent Boundary Layer Flow on a Smooth Flat Plate at Supersonic Speeds*, unclassified paper in NavOrd Rep. No. 1651 (*Confidential*), pp. 245–278, November, 1951.

[20] Monaghan, R. J., and Johnson, J. E., *The Measurement of Heat Transfer and Skin Friction at Supersonic Speeds. Part II. Boundary Layer Measurements on a Flat Plate at $M = 2.5$ and Zero Heat Transfer*, British ARC, CP No. 64, December, 1949.

[21] Rubesin, M. W., Maydew, R. C., and Varga, S. A., *An Analytical and Experimental Investigation of the Skin Friction of the Turbulent Boundary Layer on a Flat Plate at Supersonic Speeds*, NACA TN No. 2305, February, 1951.